Angewandte Chemie
Eine Zeitschrift der Gesellschaft Deutscher Chemiker

Supporting Information

Reversible Sodium Metal Electrodes: Is Fluorine an Essential Interphasial Component?

*Kyosuke Doi, Yuki Yamada, Masaki Okoshi, Junichi Ono, Chien-Pin Chou, Hiromi Nakai, and Atsuo Yamada**

anie_201901573_sm_miscellaneous_information.pdf

Author Contributions

K.D. Conceptualization: Equal; Investigation: Lead; Methodology: Equal; Writing—Original Draft: Equal
Y.Y. Conceptualization: Lead; Methodology: Equal; Supervision: Supporting; Writing—Original Draft: Equal; Writing—Review & Editing: Equal
M.O. Investigation: Supporting; Methodology: Equal; Software: Equal; Writing—Original Draft: Supporting; Writing—Review & Editing: Supporting
J.O. Investigation: Supporting; Methodology: Equal; Software: Equal
C.C. Investigation: Supporting; Methodology: Equal; Software: Equal
H.N. Resources: Equal; Software: Lead; Supervision: Supporting; Writing—Review & Editing: Equal
A.Y. Funding acquisition: Lead; Resources: Lead; Supervision: Lead; Writing—Review & Editing: Lead.

Experimental section

Materials. $NaBPh_4$ (99.5% purity) was purchased from Wako Pure Chemical Industries. $NaPF_6$, NaTFSA, DME, and conventional 1.0 M $NaPF_6$/ethylene carbonate (EC):diethyl carbonate (DEC) (1:1 by vol.) were purchased from Kishida Chemical. NaFSA was provided by Nippon Shokubai. $NaBPh_4$ was dried under vacuum at 120 °C overnight. Other materials were all of battery grade and used without further purification or pretreatment. Electrolyte solutions were prepared by dissolving the Na salts into DME at a given concentration in an Ar-filled glove box.

Electrochemical measurements. The ionic conductivity was measured by using a glass cell with a pair of platinum-plate electrodes. The cell constant was defined in advance with respect to a standard KCl aqueous solution. An electrolyte solution was put into the cell in an Ar-filled glove box, and the electrolyte bulk resistance was evaluated via the a.c. impedance method using a Solartron 147055BEC (Solartron Analytical). To study a Na plating/stripping reaction, we used a standard 2032-type coin cell with Cu foil (Fuchikawa Metal) electrode. Na metal (Wako Pure Chemical Industries) was used as a counter electrode. Glass fiber (Whatman GF/F, 420 μm thickness) was used as a separator. The volume of electrolyte was 80 μL. The coin cell was assembled with a stainless steel spacer (thickness: 0.5 mm) and a stainless steel wave washer. The pressure put on the electrodes by the wave washer was in a range of 0.1-1 MPa, which is a standard condition in the coin cell. The constant-current charge-discharge test of the Cu/Na cells was conducted using a charge-discharge unit (TOSCAT-3100, Toyo System) in a 25 °C thermostatic oven. The coin cells were charged (Na plating on Cu) for a given time and then discharged (Na stripping from Cu) up to 0.5 V. Na/Na symmetric cells (just replacing the Cu for Na in the Cu/Na coin cell) were also assembled to evaluate the stability of the Na electrode. Constant current tests were conducted at the 30 min charge-discharge time. Electrochemical impedance spectroscopy (EIS) was conducted for Na/Na symmetric cells by using a Solartron 147055BEC (Solartron Analytical). Before EIS measurements, the cells were charged and discharged at 0.5 mA cm^{-2} for 30 min to remove the surface impurity on the Na electrode.

Morphology of the plated Na. The surface morphology of the plated Na metal was analyzed by scanning electron microscopy (SEM) using an S4800 (Hitachi) at 5 kV. The Cu/Na cell was charged for 1 h at a constant current of 0.5 mA cm^{-2} and then disassembled in an Ar-filled glove box. Here, a polypropylene separator (Celgard 2400) was used with 40 μL of electrolyte because the plated Na could be more easily peeled off from this separator than the glass fiber. The plated Na metal electrode was attached to the SEM sample holder with carbon tape. The sample was transferred into an SEM chamber without being exposed to air.

Surface chemistry of Na metal. The surface chemistry of Na metal was analyzed by X-ray photoelectron spectroscopy (XPS) using a PHI 5000 VersaProbe Scanning XPS system (ULVAC-PHI) equipped with a monochromatic Al Kα X-ray source. The Cu/Na cell was charged for 1 h at

a constant current of 0.5 mA cm^{-2}, disassembled in an Ar-filled glove box, and then washed with DME solvent to minimize the amount of a residual Na salt. The washed Na metal was dried and transferred into the XPS chamber without being exposed to air. XPS spectra were obtained without Ar^+ sputtering.

Computational conditions. Electron affinities (EAs) of anions were evaluated with the B3LYP hybrid functional [1] combining Dunning's correlation-consistent double-zeta plus polarization type basis set with diffuse functions (aug-cc-pVDZ) [2-4]. Adiabatic EAs with geometric relaxation effects upon one-electron reduction were considered. Solvent effect was taken into account using the integral-equation formalism polarizable continuum model (IEFPCM) with the relative permittivity of 7.55, corresponding to DME. Convergence of geometries were confirmed with the energy difference of 0.3 meV or smaller. DFT calculations were performed using the Gaussian 16 program package [5].

The free energy surfaces (FESs) for the dissociation of $NaBPh_4$ and NaFSA ion pairs in DME were evaluated via the divide-and-conquer density-functional tight-binding molecular dynamics (DC-DFTB-MD) simulations [6,7]. The system consists of one $NaBPh_4$ (or NaFSA) and 94 (95 for NaFSA case) DME at the molarity of 0.1 M containing 1550 (1530 for NaFSA case) atoms in a cubic simulation box with three-dimensional periodic boundary condition. The DFTB3 method was employed with the 3OB parameter set [8-10].

Since the DFTB parameters for boron were not available in the 3OB parameter set, we have newly extended the parametrization using the automatized DFTB parametrization toolkit [11], in combination with the previously reported electronic parameter [12]. The resulting parameters give excellent performance as shown below.

Grimme's DFT-D3 dispersion correction with the Becke-Johnson damping scheme [13,14] was applied. The DC method with 5 × 5 × 5 Å cubic grids, resulting ca. 200 subsystems, and the buffer radius of 5 Å was employed to accelerate calculations. The equilibration and production runs were carried out under the NVT ensemble (T = 300 K) controlled by the Andersen thermostat. The velocity Verlet integrator with a time step of 1.0 fs was utilized in conjunction with the RATTLE method [15]. The well-tempered metadynamics (WTmetaD) [16] was employed to accelerate simulations. As the collective variables (CVs) of one-dimensional WTmetaD characterizing the dissociation events in $NaBPh_4$ and NaFSA, the distance between Na and B (i.e., the central atom of $[BPh_4]^-$) and that between Na and N (i.e., the central atom of $[FSA]^-$) were selected, respectively. The initial height and width of the Gaussian function for the biasing potential were set to 0.60 kcal mol^{-1} and 0.3 Å, respectively. Note that the initial Gaussian height corresponds to the thermal energy at 300 K, and the Gaussian width was obtained from the standard deviation of CV in CIP. The Gaussian biasing potential was deposited every 100 fs. The bias factor of WTmetaD was set to 15.

To analyze the effects of the structural fluctuations of solvents on the ion-pair dissociation, two-dimensional FES for CV and the coordination number between Na and DME was calculated on the basis of the reweighting method for WTmetaD [17], where the coordination number is defined as the rational form as a function of the distance [18] between Na and O atoms of DME with the cutoff distance of 3.5 Å. Here, the weighted two-dimensional histograms for CV and the coordination number were calculated from multiple biased trajectories using the reweighting method, and the resulting histograms were statistically averaged with weighted histogram analysis method (WHAM) [19]. After unbiased equilibration run for 20 ps with DC-DFTB-MD starting from the initial structure of CIP, 120 biased trajectories with different random seeds for the (stochastic) Andersen thermostat were generated from DC-DFTB-WTmetaD for 100 ps during which the weighted histograms were calculated.

DFTB parameterization for boron. The electronic parameters of boron were taken from Ref. 12. The on-site orbital energies of boron *2s* and *2p* orbitals are set to −0.3468571 and −0.1326418 a.u., respectively. The Hubbard parameter is set to 0.2962300 for both *s* and *p* orbitals. The Hubbard derivative of boron has been computed as −0.145 using PBE functional with the conventional slater-type basis with the exponents of 0.1000, 0.2659, 0.7071, 1.8803, 5.0000 and maximal power of 2. Second order confining potentials for the orbitals and density were also taken from Ref. 12, which the confining radii are 5.0 a.u. and 7.2 a.u., respectively.

The most crucial repulsive potential for this study, e.g., B-C, has been optimized specifically to reproduce the B-C bond distances of BPh_3 and $[BPh_4]^-$ molecules, along with the B-C bond dissociation energy of $[BPh_4]^-$. Although the bond dissociation will never occur in the simulation, it helps defining the proper repulsive potential depth. The reference values have been computed at B3LYP/cc-pVDZ level of theory.

The resulting parameterization gives the bond dissociation energy of 75.58 kcal mol^{-1}, which is very close to the reference value of 74.83 kcal mol^{-1}, and the B-C bond distances of the two molecules (listed in Table S1) are well reproduced. The mean absolute percentage error of the vibrational frequencies of the two molecules are also within 5% comparing to the DFT values.

Table S1. B-C bond distances of optimized BPh_3 and $[BPh_4]^-$ molecules using the new DFTB parameters, in comparison to DFT.

Molecule	Entry	DFTB3	B3LYP
BPh_3	R(B-C)[Å]	1.567	1.571
$[BPh_4]^-$	R(B-C)[Å]	1.627	1.661

Table S2. Average Coulombic efficiencies (CEs) of Na plating/stripping in various electrolytes reported in previous publications.

Electrolyte	Current density (mA cm^{-2})	Plating capacity (mAh cm^{-2})	Cycle number (-)	Ave. CE (%)
0.1 M $NaBPh_4$/DME (This work)	0.5	0.5	300	99.85
0.1 M $NaBPh_4$/DME (This work)	1	1	200	99.89
1 M $NaPF_6$/diglyme[20]	0.5	1	300	99.9 (after precycling)
4 M NaFSA/DME[21]	1	1	-	99%
2.1 M NaFSA/DME-BTFE[22]	1	1	400	98.95%
1 M NaFSA/FEC[23]	0.28	0.56	100	94%

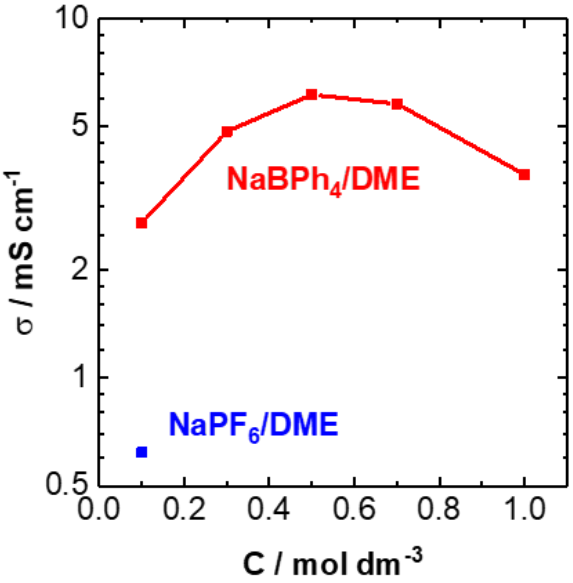

Figure S1. Ionic conductivity of DME electrolytes at various concentrations at 25 °C.

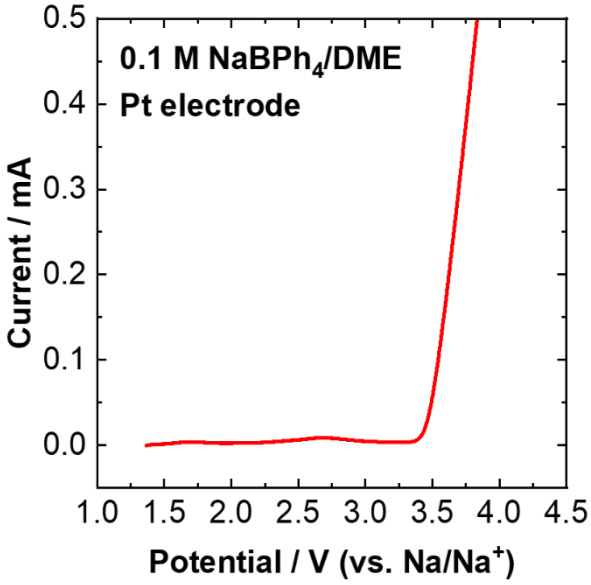

Figure S2. Linear sweep voltammogram (20 mV s^{-1}) of a Pt electrode measured in a three-electrode cell with Na metal counter and reference electrodes.

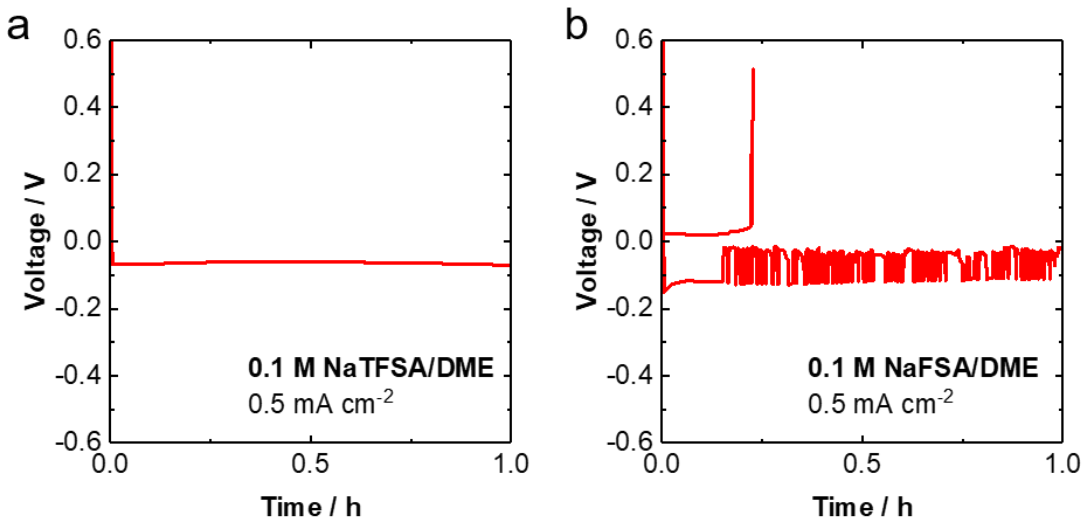

Figure S3. Charge-discharge voltage curves of a Cu/Na cell with (a) 0.1 M NaTFSA/DME and (B) 0.1 M NaFSA/DME at the constant current of 0.5 mA cm^{-2}. Na was plated on Cu for 1 h (corresponding to 0.5 mAh cm^{-2}) and then stripped up to the cut-off voltage of 0.5 V.

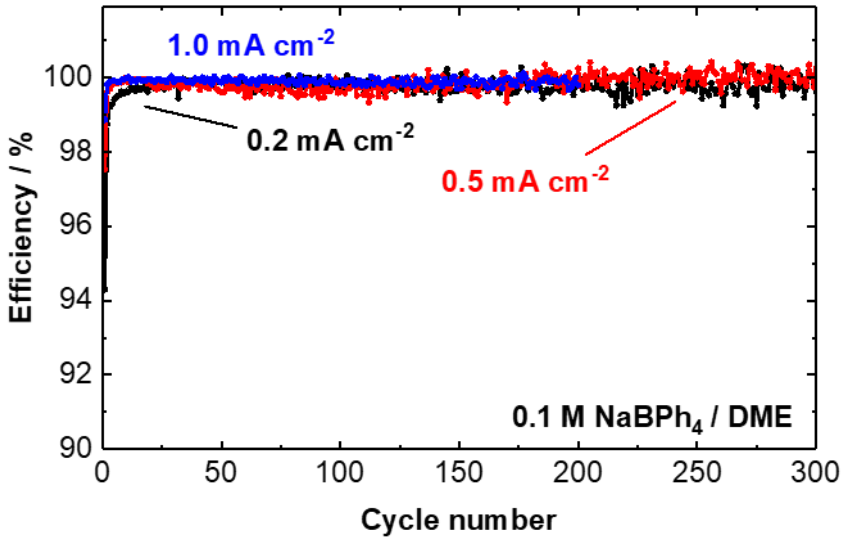

Figure S4. Coulombic efficiencies of Cu/Na cells with 0.1 M $NaBPh_4$/DME at various current densities of 0.2, 0.5 and 1.0 mA cm^{-2}. Na was plated on Cu for 1 h and then stripped up to the cut-off voltage of 0.5 V. The average Coulombic efficiency at a high current density of 1.0 mA cm^{-2} was 99.89% over 200 cycles.

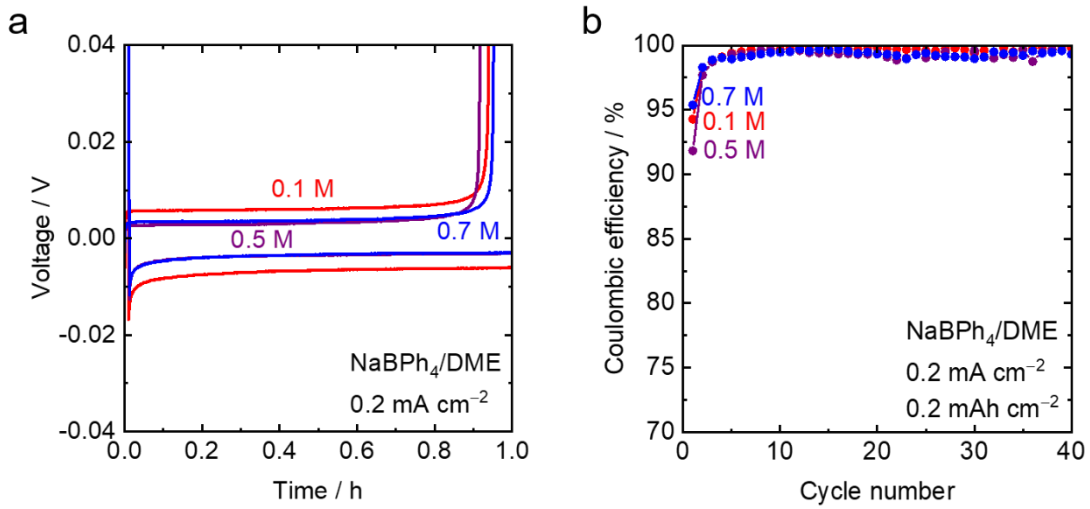

Figure S5. (a) Charge-discharge voltage curves (first cycle) of Cu/Na cells with $NaBPh_4$/DME electrolytes at various concentrations at 25 °C and a constant current of 0.2 mA cm^{-2}. Na was plated on Cu for 1 h (corresponding to 0.2 mAh cm^{-2}) and then stripped up to the cut off voltage of 0.5 V. The difference in polarization is caused primarily by their ionic conductivities. (b) Coulombic efficiencies of Na plating/stripping in the Cu/Na cells with various $NaBPh_4$/DME electrolytes.

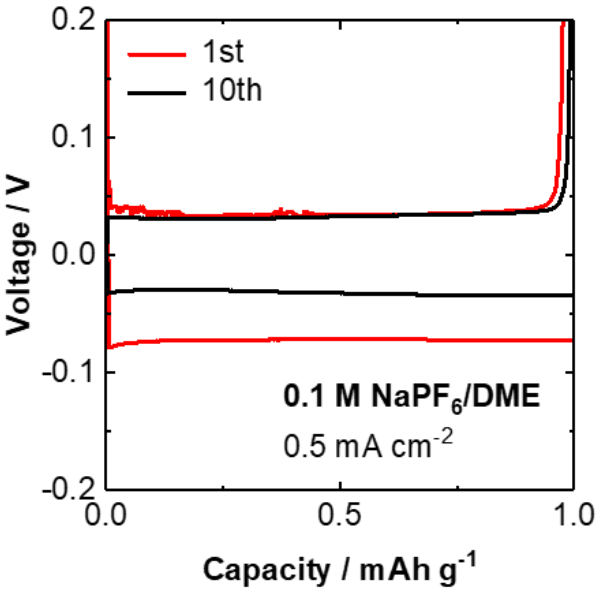

Figure S6. Charge-discharge voltage curves of a Cu/Na cell with 0.1 M $NaPF_6$/DME at the constant current of 0.5 mA cm^{-2}. Na was plated on Cu for 1 h (corresponding to 0.5 mAh cm^{-2}) and then stripped up to the cut-off voltage of 0.5 V.

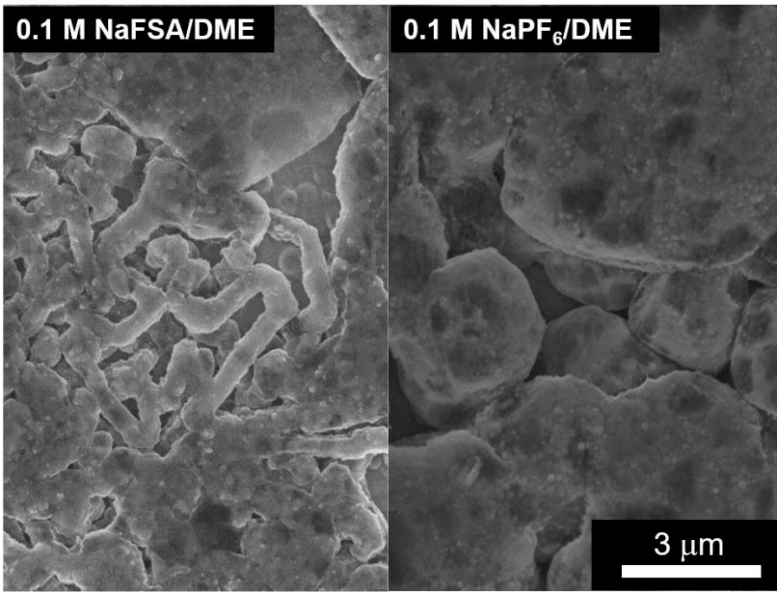

Figure S7. SEM images of the plated Na metal (corresponding to 0.5 mAh cm^{-2} at a constant current of 0.5 mA cm^{-2}) on Cu in 0.1 M NaFSA/DME and 0.1 M $NaPF_6$/DME. The plated Na in NaFSA/DME is columnar and dendritic, while that in $NaPF_6$/DME is round-shaped and large in size, which is similar to that in $NaBPh_4$/DME (Fig. 4a).

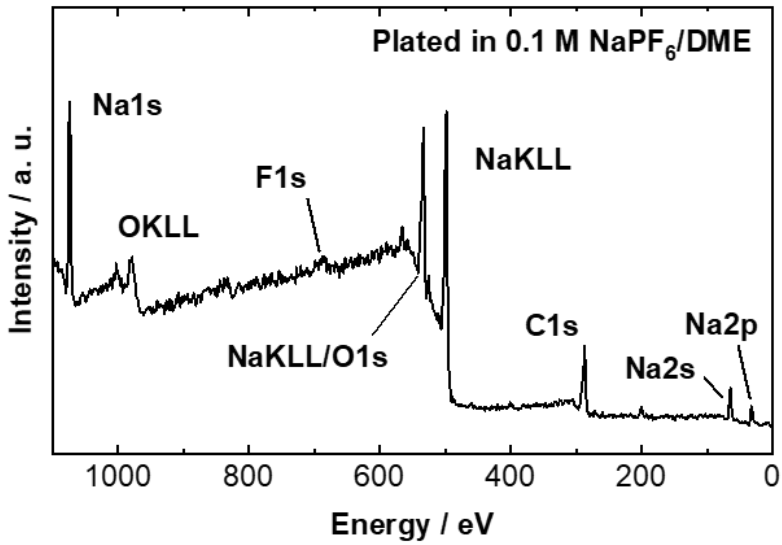

Figure S8. Wide-scan XPS spectrum of the Na metal plated in 0.1 M $NaPF_6$/DME. The surface composition is similar to that in 0.1 M $NaBPh_4$/DME, but a small amount of F-based compounds was also found.

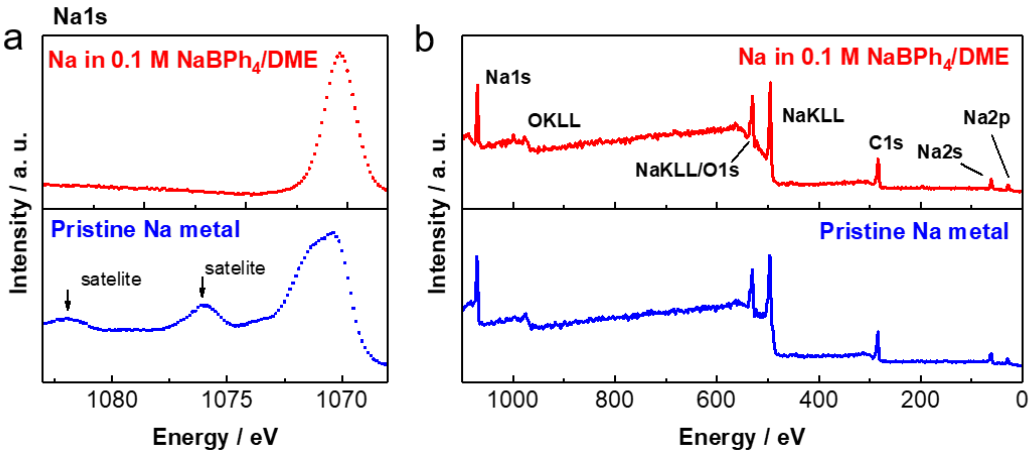

Figure S9. (a) Na1s Narrow-scan and (b) wide-scan XPS spectra of the Na metal soaked in 0.1 M $NaBPh_4$/DME for 1 h as compared to pristine Na metal.

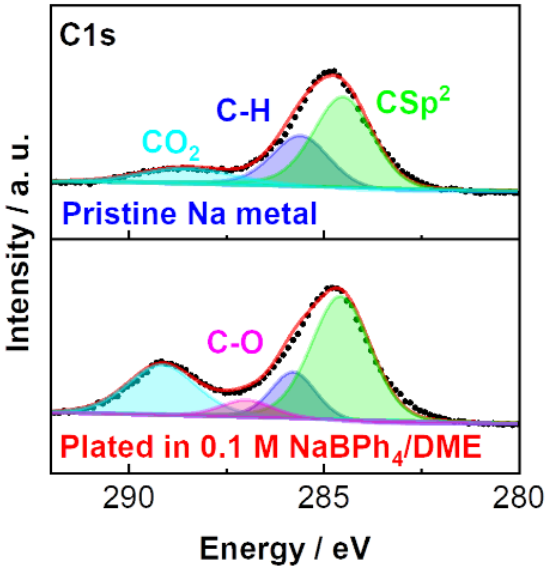

Figure S10. C1s narrow-scan XPS spectra of the Na metal plated in 0.1 M $NaBPh_4$/DME compared to pristine Na metal. A small amount of O-contained species is present on the plated Na metal. The presence of C-O was reported for the reduction products of ethers (e.g., alkoxides) [24], although we could not rule out the possibility of oxygen contaminations. Based on this result, we suppose that the surface of Na metal is stabilized due to the formation of a very thin DME-derived SEI.

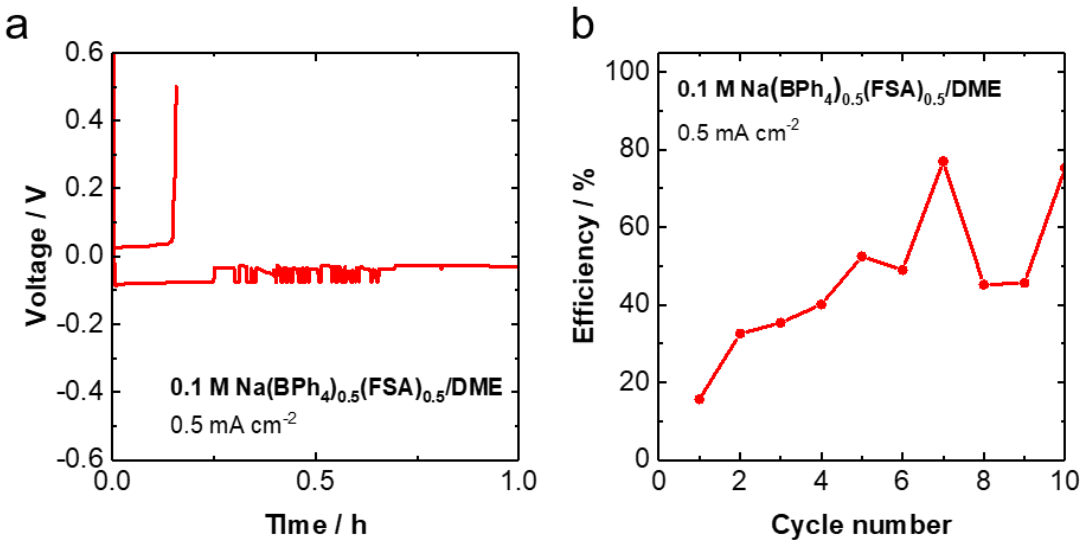

Figure S11. (a) Charge-discharge voltage curves and (b) Coulombic efficiency of a Cu/Na cell with a dual-salt system of $NaBPh_4$ + NaFSA/DME (0.05 M + 0.05 M) at the constant current of 0.5 mA cm^{-2}. Na was plated on Cu for 1 h (corresponding to 0.5 mAh cm^{-2}) and then stripped up to the cut-off voltage of 0.5 V.

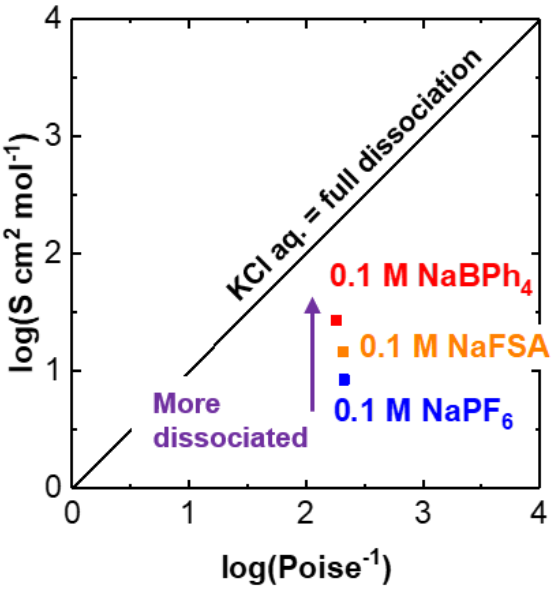

Figure S12. Walden plots of various DME solutions at 25 °C.

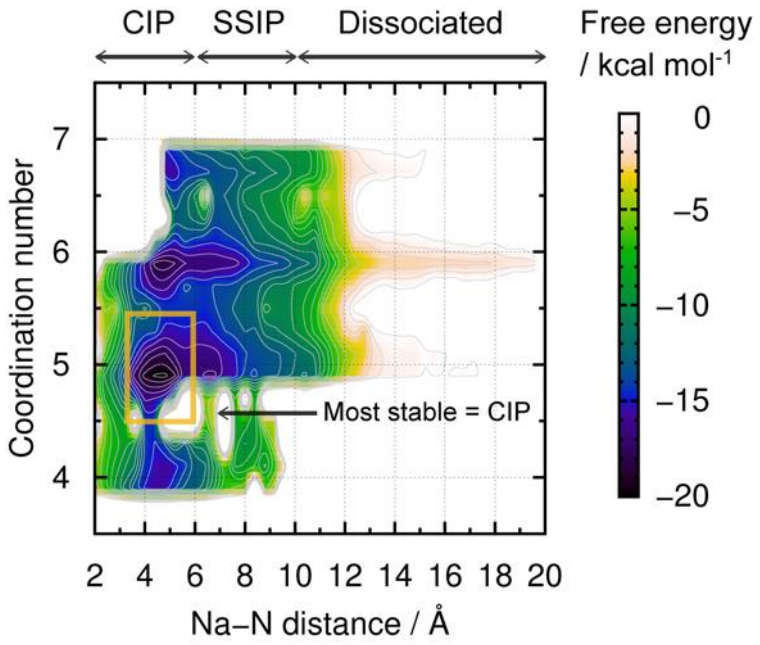

Figure S13. Two-dimensional free energy surface for the ion-pair distance and coordination number between Na and DME of NaFSA/DME solution. The probability of CIP is approximately 0.93 based on the Boltzmann distribution.

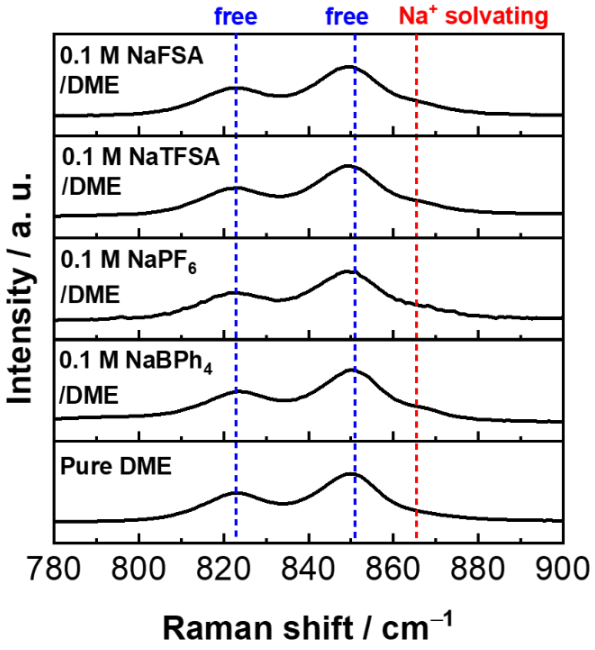

Figure S14. Raman spectra of various Na salt/DME solutions at 0.1 M concentration. The Raman bands at 823 cm^{-1} and 851 cm^{-1} are attributed to the vibration of free DME molecules with several conformers, while the band at 865 cm^{-1} is attributed to Na^+-solvating DME molecules. In these dilute electrolytes, it is difficult to analyze the solvation and ion-pair characteristics because their peaks are weak.

References for Supporting Information

1. A.D. Becke, *J. Chem. Phys.* **98**, 5648 (1993).
2. T.H. Dunning Jr., *J. Chem. Phys.* **90**, 1007 (1989).
3. R.A. Kendall, T.H. Dunning Jr., R.J. Harrison, *J. Chem. Phys.* **96**, 6796 (1992).
4. D.E. Woon, T.H. Dunning Jr., *J. Chem. Phys.* **98**, 1358 (1993).
5. Gaussian 16, M. J. Frisch, G. W. Trucks, H. B. Schlegel, G. E. Scuseria, M. A. Robb, J. R. Cheeseman, G. Scalmani, V. Barone, G. A. Petersson, H. Nakatsuji, X. Li, M. Caricato, A. V. Marenich, J. Bloino, B. G. Janesko, R. Gomperts, B. Mennucci, H. P. Hratchian, J. V. Ortiz, A. F. Izmaylov, J. L. Sonnenberg, D. Williams-Young, F. Ding, F. Lipparini, F. Egidi, J. Goings, B. Peng, A. Petrone, T. Henderson, D. Ranasinghe, V. G. Zakrzewski, J. Gao, N. Rega, G. Zheng, W. Liang, M. Hada, M. Ehara, K. Toyota, R. Fukuda, J. Hasegawa, M. Ishida, T. Nakajima, Y. Honda, O. Kitao, H. Nakai, T. Vreven, K. Throssell, J. A. Montgomery, Jr., J. E. Peralta, F. Ogliaro, M. J. Bearpark, J. J. Heyd, E. N. Brothers, K. N. Kudin, V. N. Staroverov, T. A. Keith, R. Kobayashi, J. Normand, K. Raghavachari, A. P. Rendell, J. C. Burant, S. S. Iyengar, J. Tomasi, M. Cossi, J. M. Millam, M. Klene, C. Adamo, R. Cammi, J. W. Ochterski, R. L. Martin, K. Morokuma, O. Farkas, J. B. Foresman, and D. J. Fox, Gaussian, Inc., Wallingford CT, 2016.
6. H. Nishizawa, Y. Nishimura, M. Kobayashi, S. Irle, H. Nakai, *J. Comput. Chem.* **37**, 1983 (2016).
7. Y. Nishimura, H. Nakai, *J. Comput. Chem.* **39**, 105 (2018).
8. M. Gaus, A. Goez, M. Elstner, *J. Chem. Theory Comput.* **9**, 338 (2013).
9. M. Gaus, X. Lu, M. Elstner, Q. Cui, *J. Chem. Theory Comput.* **10**, 1518 (2014).
10. M. Kubillus, T. Kubar, M. Gaus, J. Rezac, M. Elstner, *J. Chem. Theory Comput.* **11**, 332 (2015).
11. C.-P. Chou, Y. Nishimura, C.-C. Fan, G. Mazur, S. Irle, H.A. Witek, *J. Chem. Theory Comput.* **12**, 53 (2016).
12. B. Grundkötter-Stock, V. Bezugly, J. Kunstmann, G. Cuniberti, T. Frauenheim, T. A. Niehaus, *J. Chem. Theory Comput.* **8**, 1153 (2012).
13. S. Grimme, J. Antony, S. Ehrlich, H. Krieg, *J. Chem. Phys.* **132**, 154104 (2010).
14. S. Grimme, S. Ehrlich, L. Goerigk, *J. Comput. Chem.* **32**, 1456 (2011).
15. H.C. Andersen, *J. Comput. Chem.* **52**, 24 (1983).
16. A. Barducci, G. Bussi, M. Parrinello, *Phys. Rev. Lett.* **100**, 020603 (2008).
17. M. Bonomi, A. Barducci, M. Parrinello, *J. Comput. Chem.* **30**, 1615 (2009).
18. A. Laio, F.L. Gervasio, *Rep. Prog. Phys.* **71**, 126601 (2008).
19. S. Kumar, J.M. Rosenberg, D. Bouzida, R.H. Swendsen, P.A. Kollman, *J. Comput. Chem.* **13**, 1011 (1992).
20. Z. W. Seh, J. Sun, Y. Sun, Y. Cui, *ACS Cent. Sci.* **1**, 449 (2015).
21. R. Cao, K. Mishra, X. Li, J. Qian, M. H. Engelhard, M. E. Bowden, K. S. Han, K. T. Mueller,

W. A. Henderson, J.-G. Zhang, *Nano Energy* **30**, 825 (2016).

22. J. Zheng, S. Chen, W. Zhao, J. Song, M. H. Engelhard, J.-G. Zhang, *ACS Energy Lett.* **3**, 315 (2018).
23. Y. Lee, J. Lee, J. Lee, K. Kim, A. Cha, S. Kang, T. Wi, S. J. Kang, H.-W. Lee, N.-S. Choi, *ACS Appl. Mater. Interfaces* **10**, 15270 (2018).
24. Z. W. Seh, J. Sun, Y. Sun, Y. Cui, *ACS Cent. Sci.* **10**, 449 (2015).